Published in final edited form as:
Bioconjug Chem. 2010 August 18; 21(8): 1565–1570. doi:10.1021/bc1001467.

A comparison of ^{18}F PET and ^{99m}Tc SPECT imaging in phantoms and in tumored mice

Dengfeng Cheng, **Yi Wang**, **Xinrong Liu**, **P Hendrik Pretorius**, **Minmin Liang**, **Mary Rusckowski**, and **Donald J. Hnatowich**[*]
Division of Nuclear Medicine, Department of Radiology, University of Massachusetts Medical School, Worcester, Massachusetts 01655

Abstract

Our objective was to compare the performance of a microSPECT with that of a microPET in a Her2+ tumored mice using an anti-Her2 nanoparticle radiolabeled with ^{99m}Tc and ^{18}F. Camera performance was first compared using phantoms; then a tumored mouse administered the ^{99m}Tc-nanoparticle was imaged on a Bioscan NanoSPECT/CT while another tumored mouse received the identical nanoparticle, labeled now with ^{18}F, and was imaged on a Philips Mosaic HP PET camera. The nanoparticle was radiolabeled with ^{99m}Tc via MAG_3 chelation and with ^{18}F via SFB as intermediate. Phantom imaging showed that the resolution of the SPECT camera was clearly superior but even with 4 heads and multipinhole collimators, detection sensitivity was 15 fold lower. Radiolabeling of the nanoparticle by chelation with ^{99m}Tc was considerably easier and safer than manual covalent attachment of ^{18}F. Both cameras provided accurate quantitation of radioactivity over a broad range. In conclusion, when deciding between ^{99m}Tc vs. ^{18}F, an advantage rests with chelation of ^{99m}Tc over covalent attachment of ^{18}F, achieved manually or otherwise, but with these small animal cameras, this choice also results in trading lower sensitivity for higher resolution.

Keywords

Positron Emission Tomography (PET); Single Photon Emission Computed Tomography (SPECT); Computed Tomography (CT); F-18; Molecular Imaging

INTRODUCTION

While the nuclear imaging modality of choice in the clinic is often PET rather than SPECT in part because of superior sensitivity, resolution and quantitative ability, it is unclear whether the same advantages apply to small animal imaging (1–6). This investigation was conducted primarily to compare the relative spatial resolution and detection sensitivity for ^{99m}Tc on a NanoSPECT/CT camera (Bioscan Inc., Washington D.C., USA) with ^{18}F on a Mosaic HP PET (Philips Medical Systems, Inc., Cleveland, Ohio, USA). Several reports have appeared comparing radioactivity quantitation, imaging sensitivity and specificity of clinical SPECT and PET cameras in the diagnosis and monitoring of cancers and other disease states in patients (7–10). The number of comparison studies of SPECT and PET imaging of small animals using the same agent with different radiolabels is at present limited to ^{123}I and ^{124}I labeled metaiodobenzylguanidine(MIBG) for reporter gene imaging (11,12).

[*]Corresponding author: Donald J. Hnatowich, Donald.Hnatowich@umassmed.edu, Tel: 774-442-4256, Fax: 508-856-6363.

As a model radiopharmaceutical for this comparison, a delivery nanoparticle under development in this laboratory was used in which the biotinylated phosphodiamidate morpholino (MORF) oligomer (13), after radiolabeling with ^{99m}Tc or ^{18}F, was linked to the biotinylated Trastuzumab (Herceptin™) antiHer2 antibody via streptavidin as shown in scheme 1. While the radiolabeling of the nanoparticle and its biodistribution was not an objective of this investigation and although the MORF nanoparticle has been repeatedly and successfully radiolabeled with ^{99m}Tc via MAG_3 for antisense imaging (14), this report also describes the first labeling of an amine-derivitized MORF with ^{18}F. Following construction of each Trastuzumab nanoparticle by addition of the biotinylated labeled MORF both ^{99m}Tc and ^{18}F was administered to a mouse bearing Her2+ SUM190 xenografts and the animals imaged using the appropriate camera.

MATERIALS AND METHODS

General experimental

A phosphodiamidate morpholino (MORF) oligomer with the base sequence 5′-G CGTGCCTCCTCACTGGC and therefore antisense to the RIα mRNA was purchased with a biotin group on the 3′ equivalent end via a 6-aminohexanoic acid linker and a primary amine on the 5′ equivalent end (Gene Tools, Philomath, OR, USA). The S-acetyl NHS-MAG3 was synthesized in house and its structure confirmed by proton nuclear magnetic resonance and mass spectroscopy (15). The anti-Her2 Trastuzumab (Herceptin™) was obtained from Genentech Inc. (South San Francisco, CA, USA) as the clinical product. The Sulfo-NHS-LC-Biotin was purchased from Pierce (Rockford, IL, USA) and used to biotinylate the Trastuzumab antibody. Streptavidin was purchased from Sigma (St Louis, MO, USA). Standard chemicals were obtained from various suppliers and used without purification. The ^{99m}Tc pertechnetate was eluted from a ^{99}Mo-^{99m}Tc radionuclide generator (Bristol-Myers Squibb Medical Imaging Inc., North Billerica, MA, USA). The ^{18}F-fluoride was obtained on a QMA ion exchanging cartridge from PET-NET Solutions Inc. (Woburn, MA, USA). The human breast cancer cell line SUM 190 was purchased from Asterand Company (Detroit, MI, USA). Ethyl 4-(trimethylammonium)benzoate trifluoromethanesulfonate was synthesized in house following published procedures (16), and the structure confirmed by ^{1}H NMR (300 MHz, D_2O): d 1.18–1.23 (3H, t), 3.51 (9H, s), 4.20–4.27 (2H, q), 7.77–7.80 (2H, m), 8.04–8.07 (2H, m).

Preparation of N-succinimidyl-4-[^{18}F] fluorobenzoate

The amine-derivitized MORF was radiolabeled with ^{18}F via N-succinimidyl-4-[^{18}F] fluorobenzoate (^{18}F-SFB) as intermediate, selected because of its high radiochemical yield and in vivo stability (17). The synthesis of ^{18}F-SFB was achieved according to Cheng *et al*. (16).

The ^{18}F-fluoride was eluted from the QMA ion exchanging cartridge using 1.5 mL of a mixed solution of Kryptofix 2.2.2 (1–2 mg) in 0.5 mL CH_3CN and K_2CO_3 (10–12 mg) in 1 mL H_2O. Of this, 0.5 mL (7.4×10^3 MBq) was injected into a 5 ml V-vial and the solution dried azeotropically by adding 0.5 mL of CH_3CN and evaporating at 90° C under a stream of N_2. Repeating the process two more times was necessary to obtain an anhydrous product. Ethyl 4-(trimethylammonium)benzoate trifluoromethane sulfonate, 10 mg in 200 μL anhydrous CH_3CN was added to the vial containing the dried Kryptofix 2.2.2/K^+ complex of [^{18}F]F^- and the solution heated to 90° C for 5 min. The ethyl ester was then hydrolyzed by adding 0.5 mL of 1 M NaOH and heating at 90° C for 5 min, before neutralizing with 0.8 mL of 1 M HCl. The neutral solution was diluted with 2 mL H_2O and loaded onto an activated C18 Sep-Pak cartridge (Waters, Milford, MA, USA). The Sep-Pak cartridge was washed with 2 mL 0.1 M HCl to remove unlabeled ^{18}F and the 4-[^{18}F]fluorobenzoic acid

(^{18}F-FBA) was then eluted with 2 mL of CH_3CN. The HPLC analysis, performed on a Vydac 218TP C18 5 μm column (Grace, Deerfield, IL, USA) using 1:1 0.08% TFA in CH_3CN and 0.1% TFA in H_2O as eluant at 1mL/min, showed the radiochemical purity of ^{18}F-FBA to be over 98%.

To synthesize the active ester ^{18}F-SFB, tetrapropylammonium hydroxide (15 μL, 1 M in H_2O) and O-(N-succinimidyl) N,N,N′,N′-tetramethyluronium tetrafluoroborate (TSTU, 10 mg) (Sigma-Aldrich) were added to the vial containing ^{18}F-FBA in CH_3CN and the vial sealed and heated at 90° C for 5 min. Acidification was instantaneous following addition of 3 mL of 5% HOAc followed by 6 mL of H_2O. The mixture was loaded onto another activated C18 Sep-Pak cartridge. After washing with 10 mL of CH_3CN/H_2O (1:7, v/v) about 1.85×10^3 MBq of purified ^{18}F-SFB was eluted with 2 mL CH_2Cl_2. The product was identified by comparison to a stable SFB sample by HPLC as above and was also shown to be over 99% radiochemically pure including radioactivity recovery.

Preparation of the ^{18}F labeled MORF nanoparticle

The amine derivatived MORF oligomer (50 μg in 50 μl 0.3 M HEPES, pH 8.0) was added to the preparation vial containing 370 MBq ^{18}F-SFB in 20 μL CH_3CN and incubated at room temperature for 40 min with vigorously vortexing. The reaction solution containing the ^{18}F-MORF was transferred to a 0.5 ml nonstick microfuge tube with 235 μg of streptavidin in 100 μl of normal saline slowly but with vigorous mixing. Because only about half the MORF obtained from the manufacturer was biotinylated, the MORF was added to the streptavidin at a 2 fold molar excess. The mixture was incubated at room temperature for 30 min. The Trastuzumab antibody was biotinylated as previously described and added at a 1:1 molar ratio to the MORF/streptavidin (13). After incubated at room temperature for an additional 30 min, the mixture was purified on an open G75 column with 0.1 M PBS as eluant. The fractions with peak radioactivity were combined.

Preparation of the ^{99m}Tc labeled MORF nanoparticle

The amine-derivitized MORF was conjugated with NHS-MAG_3 as previously described (18). Because the preferred procedure for radiolabeling the MAG_3-MORF with ^{99m}Tc involves heating at temperatures that could potentially denature streptavidin, the MORF was again radiolabeled before adding to streptavidin. The radiolabeling of the MAG_3-MORF was achieved by adding about 407 MBq (120 μL) of ^{99m}Tc-pertechnetate generator eluant into a combined solution consisting of about 14 μg MORF in 26 μL of 0.25 M NH_4OAc, 60 μL of 100 mg/mL Na_2tartrate·$2H_2O$ in pH 9.2 labeling buffer (0.5 M NH_4HCO_3, 0.25M NH_4OAc and 0.175 M $NH_3\cdot H_2O$), and 15 μL of fresh 10 μg/μL $SnCl_2$ dissolved in pH 8.7 labeling buffer. The final pH was about 8.5. After vortexing, the mixture was incubated at room temperature for 30 min followed by incubation at 95°C for 22 min. Purification was achieved by C18 Sep-Pak chromatography in which the first elution with 0.2 M NH_4OAc removes radiolabeled pertechnetate and tartrate, the second elution with 40% CH_3CN removes radiolabeled MORF while radiolabeled colloids are retained on the cartridge.

To prepare the nanoparticle, streptavidin (12.9 μL in PBS, 64.5 μg) was added to 50 μL of PBS in a 0.5 mL nonstick microfuge tube. After vortexing, the ^{99m}Tc labeled MORF solution was slowly added at a 2:1 molar ratio (again at a molar excess to compensate for approximately half the MORF that was received without a biotin group attached) with continuous stirring. After the addition, the solution was incubated at room temperature for 30 min followed by purification on an open G75 column. Fractions of 0.5 mL each were collected. To a combined fraction containing 4 μg streptavidin, 10 μg biotinylated Trastuzumab was added at a molar ratio of 1: 1, and, after incubated at room temperature for

an additional 30 min, the product was drawn into a 1 mL U-100 Insulin Syringe for injection.

SPECT/CT and PET/CT phantom imaging

In any tomographic imaging approach, the distance of the object to be imaged from each pinhole, the diameter of the pinholes, the number of pinholes, the location of each pinhole and the number of projections all play important roles in determining detection sensitivity. In the case of the Mosaic HP PET animal camera, the detection sensitivity also depends upon the position of the object since sensitivity is maximum in the center of the FOV and decreases linearly down to zero at the edge of the FOV as more coincidences are lost when one or both of the annihilation photons escape.

Regarding resolution in pinhole SPECT imaging, the specifications of the multi-pinhole apertures, the intrinsic resolution of the crystal, the magnification employed in an imaging set up and the reconstruction settings combine to determine the reconstructed resolution. In the case of microPET imaging, in addition to the positron range that varies among PET imaging radionuclides, the reconstructed resolution depends on factors such as crystal pitch, non-collinearity of the annihilation photons caused by residual momentum of the positron, depth of interaction effects and the reconstruction methodology and settings (19).

Before proceeding to animals, resolution and detection sensitivities were compared using phantoms. To compare sensitivity, a 3 mL plastic syringe containing 18.5 MBq of ^{99m}Tc-pertechnetate in 2.5 mL H_2O was inserted into a Lucite calibration phantom (Bioscan) with an inner and outer diameter of 1 and 2 cm respectively and the phantom was placed in the mouse bed of the NanoSPECT/CT camera. Images with a pixel size of 1 mm were recorded over 360^o in 256x256 matrices with an acquisition time of 60 s per projection, resulting in a total of 24 projections per head over 30 min. The identical phantom was used to measure the PET sensitivity but with the syringe now containing 90 MBq of ^{18}F in 2.5 mL H_2O. The ^{18}F phantom was put in the center of the Field of View (FOV) of the Mosaic camera and an emission-only acquisition was obtained at a 120 mm scan length. The total scanning time was 5 min. Images of coincidence counts with a pixel size of 1 mm were recorded in 128x128 matrices.

Because of the expected differences in resolution between the cameras, two phantoms (Data Spectrum Corp., Hillsborough, North Carolina, USA) of different sizes were required. The smaller phantom used with ^{99m}Tc was provided by Bioscan and was a similar but smaller version of the Jaszczak mini hot spot phantom, with hot rods of 1.2 to 1.7 mm. The larger phantom used with ^{18}F was the Deluxe Mini Jaszczak phantom with hot rods of 1.2 to 4.8 mm. In each case the imaging protocols were similar to that described for the sensitivity measurements. The SPECT acquisition was obtained with 52 MBq of ^{99m}Tc in 24 min while the PET acquisition was obtained with 12 MBq of ^{18}F in 5 min. Using a dose calibrator (Capintec Inc., NJ, USA) and a NaI(Tl) well counter, both calibrated for counts per minute per microcurie for both radionuclides as the standard of accuracy, radioactivity quantitation on both cameras was determined with five individual measurements for identical polyethylene tubes with a dimension of 12 mm and length of 75 mm containing from 0.74 to 9.25 MBq of ^{99m}Tc or 0.37 to 12.21 MBq of ^{18}F.

SPECT/CT and PET/CT animal imaging

All animal studies were performed with approval of the UMMS Institutional Animal Care and Use Committee. Two mice (30–40g, NIH Swiss, Taconic Farms, Germantown, NY, USA) bearing SUM190 (Her2+) tumors in one thigh were used when tumor size was just below 1 cm in any dimension. One animal was injected intravenously with 0.4 μg of ^{99m}Tc-

MORF (13 MBq in 100 μl) as the MORF/Trastuzumab nanoparticle and tomographic imaging was performed at 3 and 9 h post administration on the NanoSPECT/CT camera. A CT acquisition was performed before each SPECT acquisition, at standard frame resolution, 45 kVp tube voltage and 500 ms of exposure time. About 4 min was required for each CT acquisition. The SPECT image parameters were again 1 mm/pixel, 256×256 frame size and 60 s per projection with 24 projections. Data were acquired in a step-and-shoot mode with the bed also stepping to include the whole body. Acquisition time was approximately 30 min. During imaging the animal was lightly anesthetized with 1.8% isoflurane in 1.5 L/min O_2. The CT and SPECT reconstruction was performed using InVivoScope 1.37 software (Bioscan). The CT reconstruction was at standard resolution and SPECT acquisitions were reconstructed with a voxel size of 0.4 mm using the ordered subsets Expectation Maximization (OSEM) iterative reconstruction algorithm with 4 subsets and 6 iterations. During reconstruction high noise suppression with filtering was selected to achieve smooth and more artifact-free images. Finally, the SPECT/CT fusion image was obtained using the automatic fusion feature of the software. Region-of-Interest (ROI) analysis was also obtained using InVivoScope 1.37 software. The volume of interest (VOI) was obtained in the form of a cylinder, by first circling the ROI from the transverse profile, then selecting the length of the ROI from the maximum intensity projection.

Another tumored mouse was injected intravenously with 0.4 μg of ^{18}F-MORF (0.22 MBq in 100 μl) as the identical MORF/Trastuzumab nanoparticle and PET imaging was performed at 2 and 6 h post administration on the Mosaic camera with 30 min acquisition time. The animal was lightly anesthetized during imaging as before. The PET mages were reconstructed without photon attenuation correction using the PETView program (Philips) with the fully 3D iterative reconstruction algorithm, giving a pixel size of 1 mm. Region-of-Interest (ROI) analysis was performed digitally using the Syntegra version 2.0j program (Philips). VOI was obtained from drawing the ROI in the slices of transverse profile, then interpolating the selected contours. After each PET acquisition, the mouse, immobilized on the Minerva bed (Bioscan) was transferred to NanoSPECT/CT camera for the CT acquisition and CT imaging and reconstruction was performed as before. The PET image DICOM files were transferred to the NanoSPECT/CT reconstruction workstation to provide the PET/CT fusion image.

RESULTS

Radiolabeling

The synthesis of ^{18}F-MORF and the preparation of the MORF/Trastuzumab nanoparticle required about 4 h with a final yield of 0.55 MBq labeled to 1 μg of MORF (i.e. 0.55 MBq/μg) and in a nanoparticle with 9.5 μg streptavidin and 19 μg of Trastuzumab contained in 0.3 mL PBS.

The labeling of ^{99m}Tc-MORF and the preparation of the MORF/Trastuzumab nanoparticle was accomplished in 2 h with 13 MBq labeled to 0.4 μg of MORF (i.e. 33 MBq/μg) and in a nanoparticle with 4 μg streptavidin and 10 μg of Trastuzumab contained in 0.1 mL PBS. The radiochemical purity by size exclusion HPLC of both nanoparticles was over 99% as shown by a single peak and a radioactivity recovery of 100% in both cases.

SPECT and PET phantom Imaging

The resolution obtainable by SPECT imaging of ^{99m}Tc on the NanoSPECT/CT camera and by PET imaging of ^{18}F on the Mosaic HP PET camera are illustrated in Fig. 1. By recognizing the smallest visible size of hot rods in phantoms, the tomograms provide a value

of 1.2 mm for the resolution of the SPECT image and a value of 2.4 mm for the resolution of the PET image.

While the spatial resolution of the NanoSPECT/CT camera was superior to that of the Mosaic HP PET camera, the opposite was true for sensitivity. Under conditions of this study, 2.47×10^8 counts were obtained in 5 min with 90 MBq of ^{18}F to provide a sensitivity for the Mosaic HP PET camera of 9189 cps/MBq. By comparisons, 9.88×10^6 counts were obtained in 30 min with 18 MBq of ^{99m}Tc and therefore a sensitivity of 622 cps/MBq for the NanoSPECT/CT camera, a difference of about a factor of 15. However, in considering this comparison, it is important to appreciate that while the entire phantom was within the field of view at all times during acquisition on the Mosaic HP PET camera, this was not the case during acquisition on the NanoSPECT/CT camera. Because of the motion of both the gantry and the bed during acquisition, the SPECT sensitivity varies with the position of the phantom. This is illustrated in Fig. 2 in which the average counting rate from the four heads is presented individually for each of the 24 projections. From the 10th to 20th projection, the whole phantom was in the field of view, where the four detectors can see the total radioactivity of the phantom, resulting in maximum sensitivity for these projections.

Fig. 3 shows the agreement in radioactivity quantitation between well counting and PET (top panel) and SPECT (bottom panel) imaging. In both cases, the linear regression analysis generated a coefficient of determination (R^2) of over 0.99.

SPECT and PET animal Imaging

The SPECT/CT fused images of the anterior (left panels) and left lateral (middle panels), are presented as maximum intensity projections in Fig. 4 from the 3 h (top row) and 9 h (bottom row) post injection acquisitions of one mouse. “Maximum Intensity Projections” (MIP) are defined by the manufacturer as that generated by all slices from all projections. The corresponding PET/CT fused images, also of the anterior (left panels) and left lateral (middle panels), are presented in Fig. 5 from the 2 h (top row) and 6 h (bottom row) post injection acquisitions of another mouse. All acquisitions required about 30 min.

Along with each image in both cases are presented a tomographic slice through the tumored thigh at the same level in both animals (right panels). Tumor accumulation in the left thigh is prominent in all images. Comparison of the early and late SPECT images provide evidence of rapid blood clearance, especially from the heart and carotid arteries, and slower clearance from the liver, kidneys and especially tumor. The pharmacokinetic behavior of the MORF/Trastuzumab two component nanoparticle is consistent with that previously reported for this ^{99m}Tc labeled nanoparticle (14). Comparison of the early and late PET images provides evidence of rapid blood clearance, especially from the heart and carotid arteries, and possibly slower clearance from the liver and especially tumor, although animal-to-animal differences cannot be excluded.

The percent of injected dosage in the whole body, kidneys, liver and in tumor, were estimated by quantitating the SPECT and PET acquisitions at both time points for each animal. Other organs were not included in this quantitation measurements either because of low accumulations or because of interference.

The results are presented in the histograms of Fig. 6 (SPECT) and Fig. 7 (PET). A comparison of the quantitation results show that the decay corrected whole body ^{99m}Tc radioactivity decreased from 8.66 MBq (66 % ID) to 7.28 MBq (56% ID) from 3 to 9 h while the ^{18}F radioactivity decreased from 0.16 MBq (71% ID) to 0.15 MBq (66% ID) from 2 to 6 h. The results also show similar radioactivity accumulations at both time points in tumor, however, heart and liver shows much higher radioactivity accumulations of ^{18}F.

Surprisingly, the kidney accumulations are obviously much lower in the mouse receiving the ^{18}F agent.

DISCUSSION

The superior sensitivity and excellent resolution of clinical PET compared to clinical SPECT cameras has advanced the field of nuclear medicine and the increasing availability of commercial PET clinical cameras provides opportunities to exploit new radiopharmaceuticals labeled with PET radionuclides for oncologic, cardiac, neurologic, etc. imaging (3). However, the large difference in subject size between human patients and small animals requires a different physics for the optimization of cameras performance. We therefore asked whether the advantages of PET over SPECT tomographic imaging in the clinic extend to the imaging of small animals such as tumored mice. Although not the object of this investigation, because of differences in camera performance, we also asked whether labeling our delivery nanoparticle with ^{18}F would offer advantages over labeling with ^{99m}Tc. Because of the large size of the nanoparticle, the pharmacokinetics was expected to be largely radiolabel independent.

Apart from camera performance, there clearly are advantages to radiolabeling with ^{99m}Tc, usually the preferred SPECT radionuclide, compared to radiolabeling with ^{18}F, often the preferred PET radionuclide (20–22). For those radiopharmaceuticals not commercially available and therefore requiring in-house preparation, radiolabeling by chelation with ^{99m}Tc will in all cases require less time and effort and less personnel exposure than radiolabeling with ^{18}F. Use of a remote ^{18}F automated synthesis apparatus would significantly increase the efficiency of the synthesis and decrease personal exposure but the effort would still not approach the simplicity of chelation labeling as shown in this research in the labeling of the MORF oligomer with ^{99m}Tc and ^{18}F. To our knowledge, this investigation is the first to compare the Bioscan NanoSPECT/CT and Philips Mosaic HP PET cameras by imaging mice administered the same agent but with different radiolabels.

We recognize that arriving at a meaningful comparison between PET and SPECT imaging is complicated by the distinctly different detection physics involved. Regarding camera performance, whereas clinical PET cameras are reported to provide superior spatial resolution compared to SPECT cameras at least in the case of PET radionuclides such as ^{18}F with relatively low maximum beta energies, the opposite was found to be the case for the small animal cameras of this investigation. A comparison of the PET and SPECT phantom images in Fig. 1 clearly shows the latter to provide superior spatial resolution. The NanoSPECT is a conventional gamma camera configured as a small animal imaging system using, in this case, four multi-pinhole aperture plates each with 9 pinholes of 1.4 mm rather than conventional parallel hole or fan-beam collimators. The superior spatial resolution is also evident in a comparison of the whole body images shown in Figs. 4 and 5. However, in agreement with the experiences with clinical cameras, the higher detection sensitivity of PET cameras extended to small animal cameras as well. Under the conditions of this study, two sources positioned in identical geometry in both cameras provided approximately 15 fold higher counts in the Mosaic HP PET camera compared to the NanoSPECT/CT camera. Accordingly, the images of Figs. 4 and 5 were obtained in animals injected with 13 MBq of ^{99m}Tc and only 0.22 MBq of ^{18}F requiring 30 min for both SPECT and PET acquisition.

Since this investigation was more concerned with comparing camera performance than with comparing the pharmacokinetics of the two radiolabeled nanoparticles, only two tumored mice were imaged, relying upon the results of the phantoms studies to compare resolution, sensitivity and accuracy. Accordingly, the animal results are subject to uncertainties related to animal-to-animal variations. This may explain the small but important differences

observed in the pharmacokinetics of the two nanoparticles. While tumor accumulations were identically high due to the targeting of the Her2+ SUM190 xenografts by the antiHer2 antibody within each nanoparticle, accumulations of ^{18}F were higher in blood (heart) and liver at both time points. These differences were unexpected since the large size of the nanoparticle was expected to mask small differences in chemical properties related to the different labeling methods.

CONCLUSIONS

Radiolabeling of the MORF oligomer within the nanoparticle by chelation with ^{99m}Tc was considerably more efficient than radiolabeling with ^{18}F via the manual synthesis with ^{18}F-SFB. Thus when deciding between ^{99m}Tc vs. ^{18}F as the radiolabel for the nanoparticle (and other similar biomolecules) for imaging on the NanoSPECT/CT and Mosaic HP PET small animal imaging cameras, while an advantage rests with chelation of ^{99m}Tc over covalent attachment of ^{18}F, the choice of ^{99m}Tc trades lower sensitivity for higher resolution.

Acknowledgments

The authors are grateful to Dr. Jack Hoppin (Bioscan Inc., Washington D.C.) for his valuable comments. This research was supported in part by the National Institutes of Health (S10 RR023066).

LITERATURE CITED

1. Culver J, Akers W, Achilefu S. Multimodality Molecular Imaging with Combined Optical and SPECT/PET Modalities. J Nucl Med. 2008; 49:169–172. [PubMed: 18199608]
2. Herschman HR. Micro-PET imaging and small animal models of disease. Curr Opin Immunol. 2003; 15:378–384. [PubMed: 12900267]
3. Seo Y. Quantification of SPECT and PET for Drug Development. Current Radiopharmaceuticals. 2008; 1:17–21.
4. Liang H, Yang Y, Yang K, Boone JM, Cherry SR. A microPET/CT system for in vivo small animal imaging. Phys Med Biol. 2007; 52:3881–3894. [PubMed: 17664583]
5. Lundqvist H, Tolmachev V. Targeting Peptides and Positron Emission Tomography. Biopolymers (Peptide Science). 2002; 66:381–392. [PubMed: 12658725]
6. Chatziioannou AF. Instrumentation for Molecular Imaging in Preclinical Research Micro-PET and Micro-SPECT. Proc Am Thorac Soc. 2005; 2:533–536. [PubMed: 16352760]
7. Eshuis A, Jager PL, Maguire RP, Jonkman S, Dierckx RA, Leenders KL. Direct comparison of FP-CIT SPECT and F-DOPA PET in patients with Parkinson's disease and healthy controls. Eur J Nucl Med Mol Imaging. 2009; 36:454–462. [PubMed: 19037637]
8. Vlasenko A, Petit-Taboué M, Bouvard G, Morello R, Derlon J. Comparative quantitation of cerebral blood volume: SPECT versus PET. J Nucl Med. 1996; 38:919–924. [PubMed: 9189142]
9. Bremner JD, Baldwin R, Horti A, Staib LH, Ng CK, Tan PZ, Zea-Ponce Y, Zoghbi S, Seibyl JP, Soufer R, Charney DS, Innis RB. Quantitation of benzodiazepine receptor binding with PET [^{11}C]iomazenil and SPECT [^{123}I]iomazenil: preliminary results of a direct comparison in healthy human subjects. Psychiatry Res. 1999; 91:79–91. [PubMed: 10515463]
10. Even-Sapir E, Metser U, Mishani E, Lievshitz G, Lerman H, Leibovitch I. The Detection of Bone Metastases in Patients with High- Risk Prostate Cancer: ^{99m}Tc-MDP Planar Bone Scintigraphy, Single- and Multi-Field-of-View SPECT, ^{18}F-Fluoride PET, and ^{18}F-Fluoride PET/CT. J Nucl Med. 2006; 47:287–297. [PubMed: 16455635]
11. Doubrovin MM, Doubrovina ES, Zanzonico P, Sadelain M, Larson SM, O'Reilly RJ. In vivo Imaging and Quantitation of Adoptively Transferred Human Antigen-Specific T Cells Transduced to Express a Human Norepinephrine Transporter. Gene Cancer Res. 2007; 67:11959–69.
12. Moroz MA, Serganova I, Zanzonico P, Ageyeva L, Beresten T, Dyomina E, Burnazi E, Finn RD, Doubrovin M, Blasberg RG. Imaging hNET Reporter Gene Expression with ^{124}I-MIBG. J Nucl Med. 2007; 48:827–836. [PubMed: 17475971]

13. Liu X, Wang Y, Nakamura K, Kubo A, Hnatowich DJ. Cell studies of a three-component antisense MORF/tat/Herceptin nanoparticle designed for improved tumor delivery. Cancer Gene Therapy. 2008; 15:126–132. [PubMed: 18084241]

14. Wang Y, Liu X, Chen L, Rusckowski M, Hnatowich DJ. Tumor delivery of antisense oligomer using trastuzumab within a streptavidin nanoparticle. Eur J Nucl Med Mol Imaging. 2009; 36:1977–1986. [PubMed: 19572130]

15. Wang Y, Liu X, Hnatowich DJ. An improved synthesis of NHS-MAG3 for conjugation and radiolabeling of biomolecules with ^{99m}Tc at room temperature. Nat Protoc. 2007; 2:972–978. [PubMed: 17446896]

16. Cheng D, Yin D, Zhang L, Wang M, Li G, Wang Y. Preparation of the novel fluorine-18-labeled VIP analog for PET imaging studies using two different synthesis methods. J Fluorine Chem. 2007; 128:196–201.

17. Wester HJ, Hamacher K. Stöcklin, G. A. Comparative study of N.C.A. Fluorine-18 labeling of protein via acylation and photochemical conjugation. Nucl Med Biol. 1996; 23:365–372. [PubMed: 8782249]

18. Wang Y, Nakamura K, Liu X, Kitamura N, Kubo A, Hnatowich DJ. Simplified Preparation via Streptavidin of Antisense Oligomers/Carriers Nanoparticles Showing Improved Cellular Delivery in Culture. Bioconjugate Chem. 2007; 18:1338–1343.

19. Levin CS, Hoffman EJ. Calculation of positron range and its effect on the fundamental limit of positron emission tomography system resolution. Phys Med Biol. 1999; 44:781–799. [PubMed: 10211810]

20. Stöcklin GL. Is there a future for clinical fluorine-18 radiopharmaceuticals (excluding FDG)? Eur J Nucl Med. 1998; 25:1612–1616. [PubMed: 9917190]

21. Okarvi SM. Recent progress in fluorine-18 radiopharmaceuticals. Eur J Nucl Med. 2001; 28:929–938. [PubMed: 11504093]

22. Cai L, Lu S, Pike VW. Chemistry with [^{18}F]Fluoride Ion. Eur J Org Chem. 2008; 17:2853–2873.

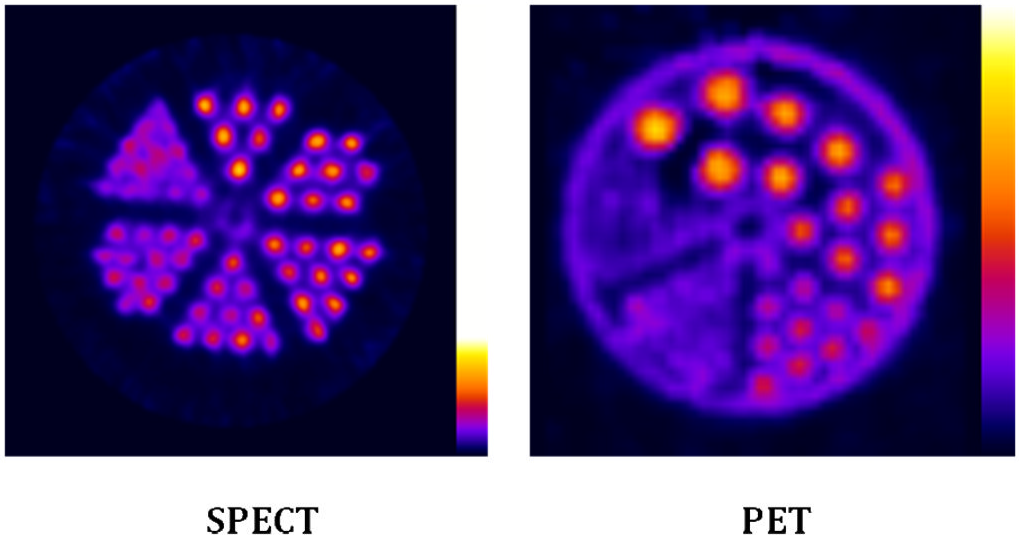

Fig. 1.

A tomographic image of a phantom with hot rods of 1.2 mm to 1.7 mm obtained on the NanoSPECT/CT small animal imaging camera (left panel) and a tomographic image of another phantom with hot rods of 1.2 mm to 4.8 mm obtained on the Mosaic HP PET (right panel) small animal imaging camera.

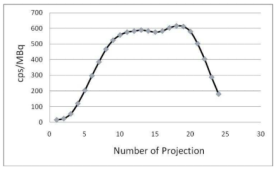

Fig. 2.

Detection sensitivity in cps/MBq vs. projection number showing variation due to the motion of both the gantry and the animal bed during imaging on the NanoSPECT/CT camera.

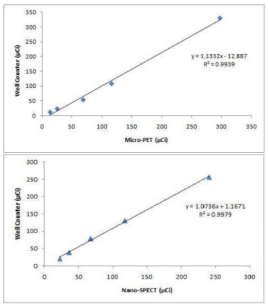

Fig. 3.

Radioactivity quantitation comparison between well counting and PET (top panel) and SPECT (bottom panel) imaging. Solid line connecting data points drawn by a linear regression analysis.

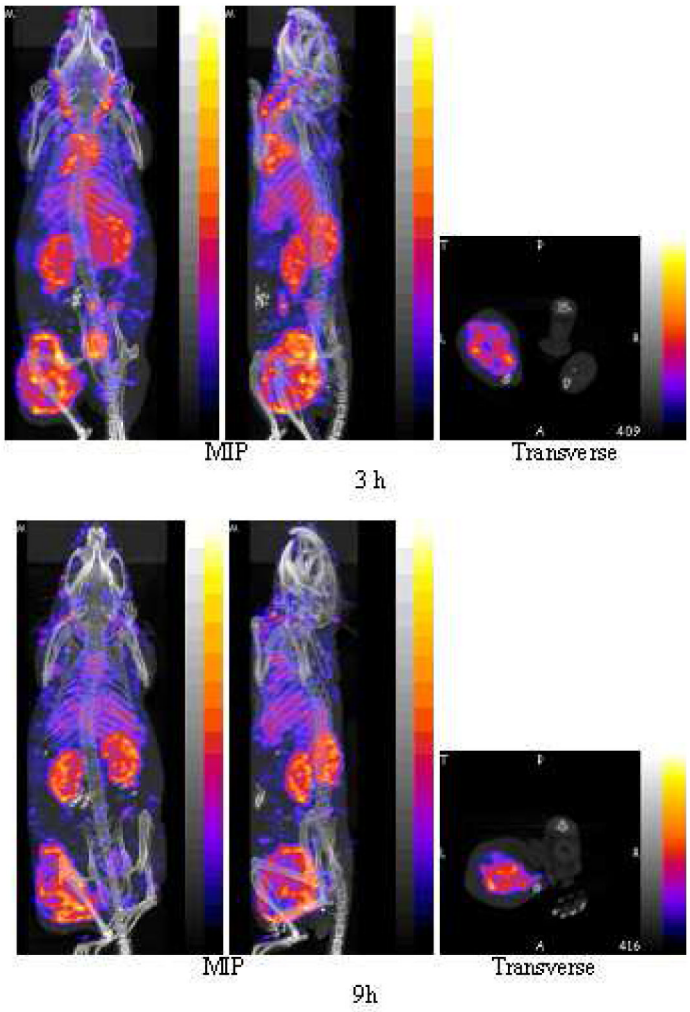

Fig. 4.

SPECT and fused CT projections obtained by imaging one mouse bearing a SUM190 tumor in the left thigh at 3 h (top row) and again at 9 h (bottom row) post injection of 100 μL (13 MBq) of ^{99m}Tc labeled nanoparticle with each acquisition requiring 30 min. Each row presents an anterior (left panel) and left lateral projection (middle panel), both Maximum Intensity Projections (MIP) and a transverse slice (right panel) of the acquisition centered on the tumor.

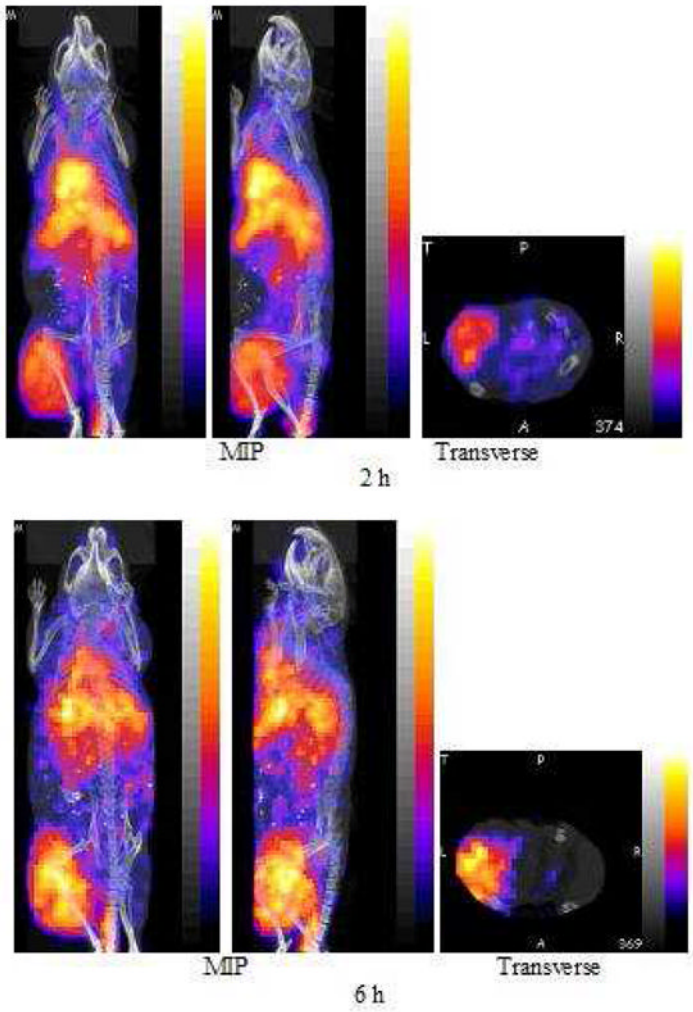

Fig. 5.

PET and fused CT projections obtained by imaging one mouse bearing a SUM190 tumor in the left thigh 2 h (top row) and again at 6 h (bottom row) post injection of 100 μL (0.22 MBq) of ^{18}F labeled nanoparticle with each acquisition requiring 30 min. Each presents an anterior (left panel) and left lateral projection (middle panel), both Maximum Intensity Projections (MIP) and a transverse slice (right panel) of the acquisition centered on the tumor.

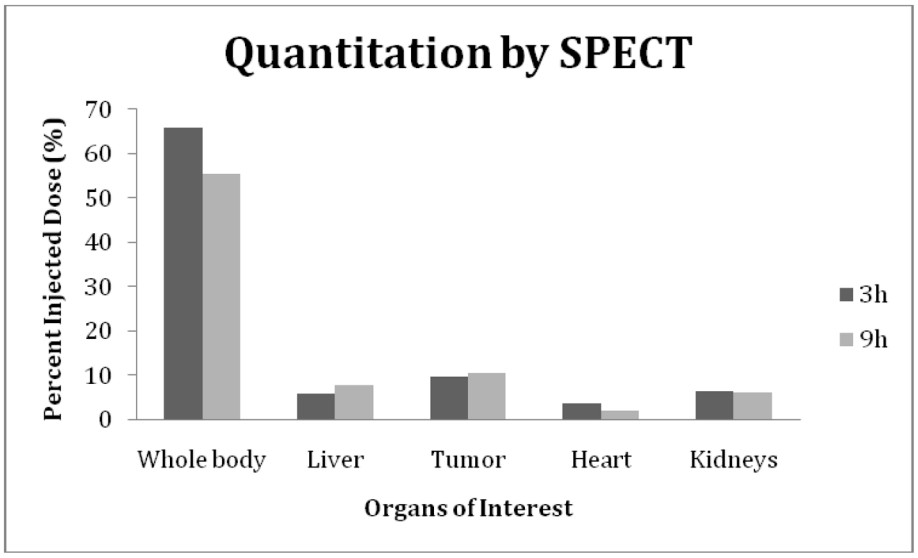

Fig. 6.

The percent injected dose (%ID) in the whole body, tumor and three normal organs at 3 and 9 h post administration of the ^{99m}Tc-MORF/Trastuzumab nanoparticle to a tumored mouse. Radioactivity quantitation was accomplished by using InVivoScope software.

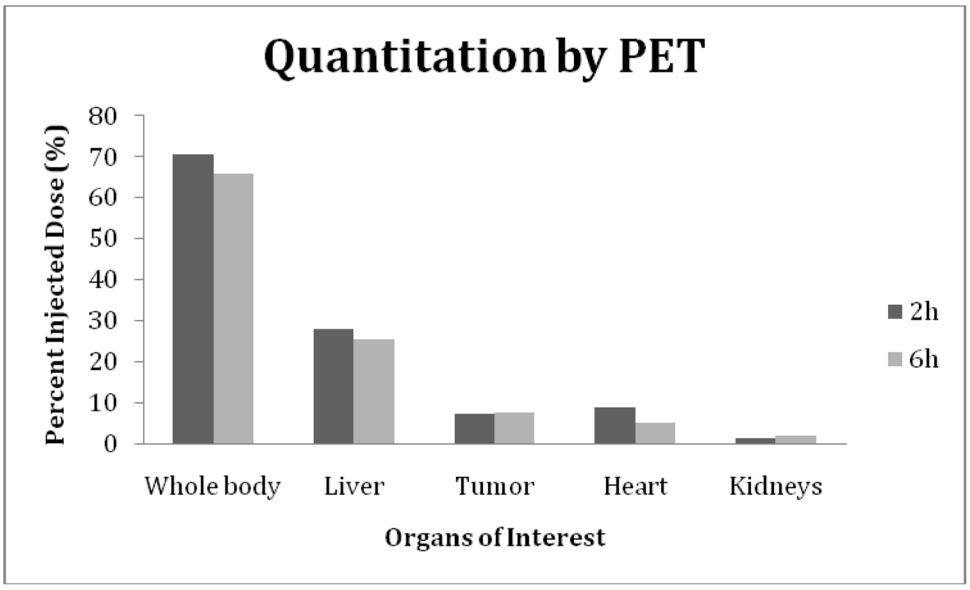

Fig. 7.

The percent injected dose (%ID) in the whole body, tumor and three normal organs at 2 and 6 h post administration of the ^{18}F-MORF/Trastuzumab nanoparticle to a tumored mouse. Radioactivity quantitation was accomplished by using Syntegra version 2.0j program.

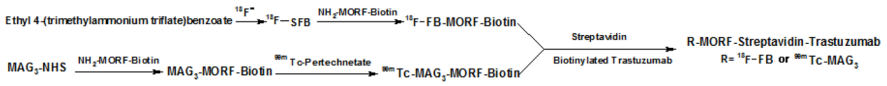

Scheme 1.
Showing the preparation scheme for ^{99m}Tc and ^{18}F labeling streptavidin nanoparticles.